A Linear Synchronous-Motor Model for Evaluation of Sensorless Methods

Roberto Leidhold and Peter Mutschler
Darmstadt University of Technology, Germany.
rleidhold@ieee.org, pmu@srt.tu-darmstadt.de

***Abstract*- In this work, a model for the Long-Stator Linear Synchronous-Motor is derived. The purpose of this model is the evaluation of sensorless control methods. The model is composed by a magnetostatic and an electrical subsystem. The magnetostatic subsystem is derived by using the Magnetic Equivalent Circuit (MEC) and is expressed as a set of implicit nonlinear algebraic equations. The electrical subsystem is coupled with the former and is expressed by a set of ordinary differential equations. The complete model is solved with a numerical method for Differential Algebraic Equations (DAE). The MEC is derived from the motor geometry, magnetic characteristics of the involved materials, and the winding arrangement. This allows doing analysis and simulation of a motor before it is build. In this work, an existing Long-Stator Synchronous-Motor is modeled. First, the magnetostatic subsystem is compared with Finite Element Analisys (FEA), and second, the complete model is validated with experimental results.**

I. INTRODUCTION

An important number of sensorless methods have been proposed for rotative motors [1][2], however few works can be found applying it for linear motors e.g. [3]. Linear motors present additional challenges to be solved for the implementation of sensorless methods, as like as asymmetries caused by end effects, or non-periodicity of the flux linkage or of the saliencies. Moreover, long-stator motors are usually split in several segments to allow multiple movers and reducing the reactive power (e.g. Transrapid), but making the implementations of sensorless techniques more complex. It is also to be considered that there is a higher diversity of linear motors than rotative ones, requiring a targeted analysis for each case.

The first step for implementing a sensorless control method is to have an adequate model. When the motor is still under development and there isn't a prototype available to get the model parameters by experimental tests, the Finite Element Analysis (FEA) is the usual tool. In [4] the use of FEA is proposed for analyzing the ability to implement a sensorless method on a motor. The FEA is however very time-consuming making it inadequate for a dynamic simulation. Another alternative is to use the Magnetic Equivalent Circuit (MEC) method [5], which can also be implemented starting from the motor geometry and magnetic characteristics of the involved materials.

In the present work, a MEC based model is proposed to be used to evaluate sensorless methods on linear motors. The model is composed by a magnetostatic and an electrical subsystem. The magnetostatic subsystem is derived by using the MEC and is expressed as a set of implicit nonlinear algebraic equations. The electrical subsystem is coupled with the former and is expressed by a set of ordinary differential equations. The complete model is solved with a numerical method for Differential Algebraic Equations (DAE).

A Long Stator Synchronous Motor, available in the authors institute, is modeled. In order to validate the proposed model, in a first instance the magnetostatic subsystem is compared with FEA, and in a second instance, the complete model is validated with experimental results.

This paper is organized as follows: In Section II the long-stator linear synchronous-motor is described. In Section III the MEC based model is elaborated. In Section IV results of comparing the model with FEA and experimental tests are presented. Finally, in Section V, some conclusions are drawn.

II. MOTOR GEOMETRY

The Long Stator Synchronous Motor is arranged in multiple segments i.e. stators. Each segment is composed by two facing stator-sides forming a slot between them where the mover translates. The windings of both sides are parallel-connected and electrically independent from the other segments. In Fig. 1 the diagram of one segment of the motor is shown.

In this figure, the geometry of the stator and the mover as well as the winding distribution is shown. Each segment has 13 poles arranged in 39 slots, while the mover has 3 poles.

III. MODEL

A. Magnetostatic subsystem

The model of the magnetostatic subsystem is derived by using the Magnetic Equivalent Circuit (MEC) method [5]. By modeling the magnetic system only statically, effects like Eddy currents will not be considered. Even if some sensorless methods rely on high frequency injection, it analysis can be well done neglecting Eddy current effects, e.g. [4]. Other methods, however, are expressly based on the transient inductance [6], which would not be well modeled with only a magnetostatic analysis.

The MEC method consists in dividing the magnetic system in pieces in which the flux flows in (almost) one direction [5].

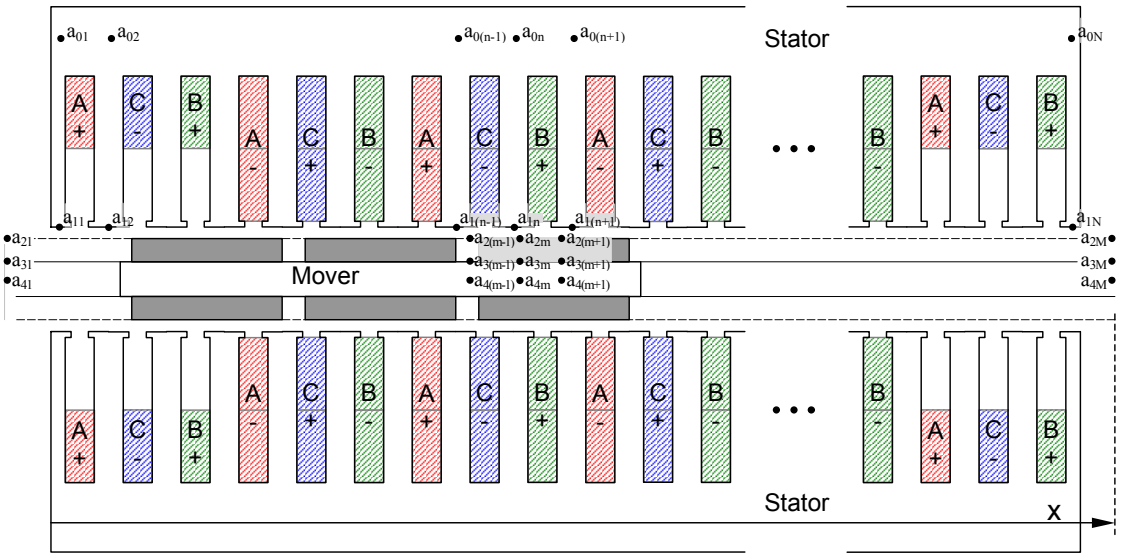

Fig. 1 Diagram of the PM Linear Motor Geometry

These pieces, also called "flux tubes", are represented in the Equivalent Circuit by resistances, characterizing the magnetic reluctance (or permeance). Windings are represented in the equivalent circuit by controlled Magneto-Motive-Force (MMF) sources. While Permanent Magnets (PM) are represented by constant flux sources.

The motor of Fig. 1 can be modeled with the equivalent circuit shown in Fig. 3. Fluxes are designated by ϕ, magneto-motive-forces by F, reluctances by R (permeances by g) and the Magnetic Potential at node $\{i, j\}$ by a_{ij}. The magnetic potential at each node in Fig. 3 is related to the corresponding points shown in the diagram of Fig. 1. The equivalent circuit uses N = 40 branches representing stator teeth, while the mover is divided into M = 222 branches representing virtual teeth of the actual mover and the air slice between both stator sides where the mover is absent.

The lower half of the mover and the lower stator are even-symmetric to it upper counterparts. In the case of FEA simulation, it is used to take advantage of this kind of symmetry by simulating only one half of the system, and using symmetry boundary conditions. Similarly, in the MEC this boundary condition can be implemented by shorting together all nodes laying on the axis of symmetry as shown in the circuit of Fig. 3.

Leakage, yoke and mover-tooth reluctances (R_{SL}, R_{MLm}, R_{SY}, R_{Mam} and R_{Mbm}) are linear. Only the stator tooth reluctance R_{ST} is considered inherently nonlinear, as there is where the flux density is higher. The airgap reluctances $R_{Gm,n}$, which relate each node of layer 1 with each node of layer 2, are parametric nonlinear, depending on the mover position x. The airgap permeance g_G between stator tooth 1 and mover tooth 1 can be calculated as,

$$g_G = \frac{\mu_0 \, l_S \, b_G(x)}{g} \qquad (1)$$

where $b_G(x)$ is the airgap length covered simultaneously by both teeth, g is the airgap height, μ_0 is the air permeability and l_S is the stack height. The function $b_G(x)$ is implemented by spline interpolation from the points shown in Fig. 2, where b_{ST} and b_{MT} are the stator and mover tooth width respectively. In the same figure, the resulting curve is shown with dashed line. For the remaining teeth, the function $b_G(x)$ is shifted by the distance between them.

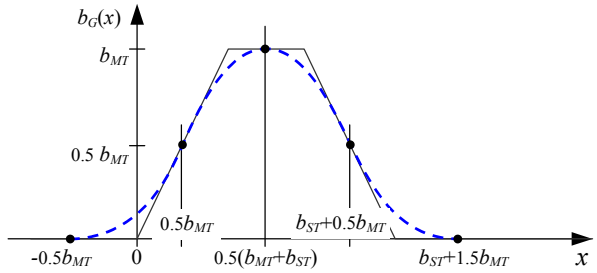

Fig. 2 Function $b_G(x)$ (airgap length covered simultaneously by both teeth)

In order to solve the MEC, the corresponding node and potential equations are derived and expressed as an implicit function:

$$0 = \mathbf{f}_1\left(\mathbf{F_S}, \mathbf{a_0}, \mathbf{a_1}, \mathbf{a_2}, \mathbf{a_3}, a_4, \boldsymbol{\varphi_S}, x\right) \qquad (2)$$

Where matrix and vectors are designated by bold symbols, $\mathbf{a}_0$ to a_4 are the potential vectors of each layer, $\boldsymbol{\varphi_S}$ is the stator teeth flux vector, $\mathbf{F_S}$ is the teeth MMF vector, and x the mover's position. The implicit function (2) has 3xN+2xM rows, 3xN+2xM unknown variables and N+1 known variables (e.g. N = 40; M = 222). The complete expression of (2) is presented in Appendix I.

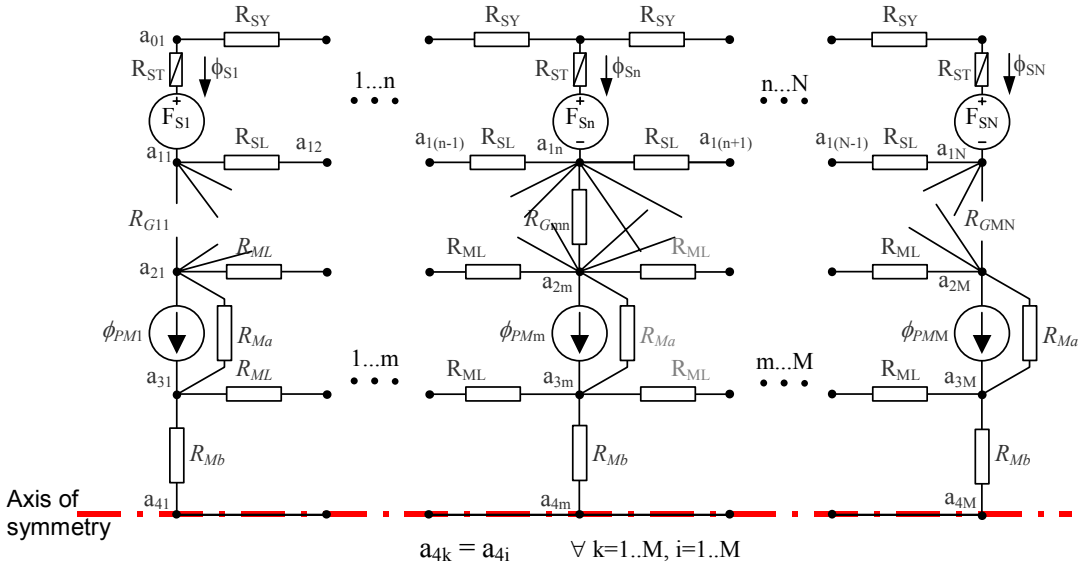

Fig. 3 Magnetic Equivalent Circuit of the Linear Motor of Fig. 1

In order to interface the magnetostatic subsystem with the electric subsystem, the teeth MMF vector $\mathbf{F_S}$ is related with the phase currents as follows,

$$\mathbf{F_S} = \mathbf{w}''_S \, \mathbf{i}_S \tag{3}$$

where $\mathbf{i}_S = [i_A \; i_B \; i_C]^T$ is the phase current vector, and $\mathbf{w}''_S$ is the MMF transformation matrix, which can be derived from the winding distribution [5]. Similarly, the flux linkage can be related with the teeth flux vector $\boldsymbol{\varphi}_\mathbf{S}$ by,

$$\boldsymbol{\lambda}_\mathbf{S} = \mathbf{w}'_\mathbf{S} \, \boldsymbol{\varphi}_\mathbf{S} \tag{4}$$

where $\boldsymbol{\lambda}_\mathbf{S} = [\lambda_A \; \lambda_B \; \lambda_C]^T$ is the phase flux linkage vector, and $\mathbf{w}' = \mathbf{w}''^T$.

Substituting (3) and (4) into (2), and solving the invariant linear subsystem, it can be reduced to,

$$0 = \mathbf{f}_2\left(\mathbf{i_S}, \mathbf{a_1}, \mathbf{a_2}, \boldsymbol{\lambda}_\mathbf{S}, x\right) \tag{5}$$

Shrinking to N+M+3 rows, N+M+3 unknown variables and 3+1 known variables.

B. *Electric subsystem*

The linear motor is fed by a voltage source inverter. In Fig. 4, the electric circuit of such a system is shown. Even when the star point is not connected, the inclusion of a high resistance R_N is considered to get the star point voltage u_{N0} in the simulation. It is included in this work, as several sensorless methods are based on measuring this voltage.

From the circuit of Fig. 4 the complete set of differential equations can be derived,

$$d\boldsymbol{\lambda}_\mathbf{S} / dt = -\mathbf{R}\,\mathbf{i_S} + \mathbf{u} \tag{6}$$

with,

$$\mathbf{R} = \mathbf{I_3}\, R + \mathbf{1}_{3x3}\, R_N \tag{7}$$

being $\mathbf{I_3}$ the identity matrix, and $\mathbf{1}_{3x3}$ a 3x3 matrix of ones.

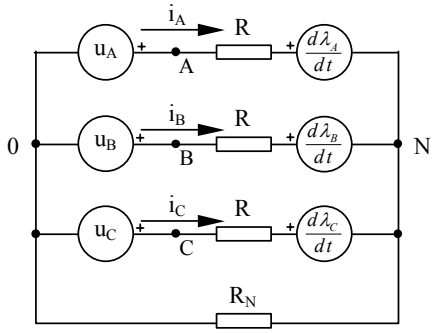

Fig. 4 Electrical circuit of the linear drive

C. *Complete system*

The set of implicit nonlinear algebraic equations (2) cannot be directly solved in order to insert it in the differential equation (6) i.e. cannot be expressed as $\mathbf{i_S} = \mathbf{f}(\boldsymbol{\lambda}_S)$. Consequently, it must be solved numerically together with the differential equation. Equations (6) and (5) form a set of differential algebraic equations (DAE). In order to solve the DAE, the algorithm presented in [7] is used. In order to start solving the DAE, consistent initial states must be provided. Therefore, the algebraic equation will be solved first (with the initial states of the ODE, $\boldsymbol{\lambda}_\mathbf{S}(0)$), using a nonlinear algebraic solver.

IV. Results

A. *Magnetostatic MEC simulations compared with FEA*

The sensorless capability of a synchronous motor can be initially analyzed from the position dependence of its inductance or its induced Electro Motive Force (EMF), depending on the considered sensorless method. The inductance matrix was derived as a function of the position and

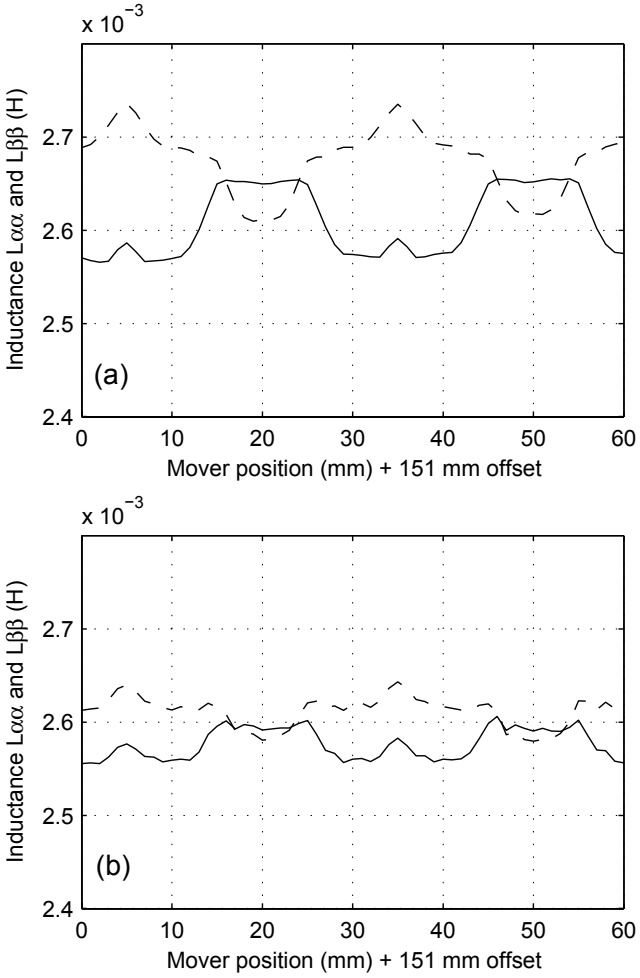

Fig. 5 Inductance Lαα as a function of the position, a) by MEC, b) by FEA

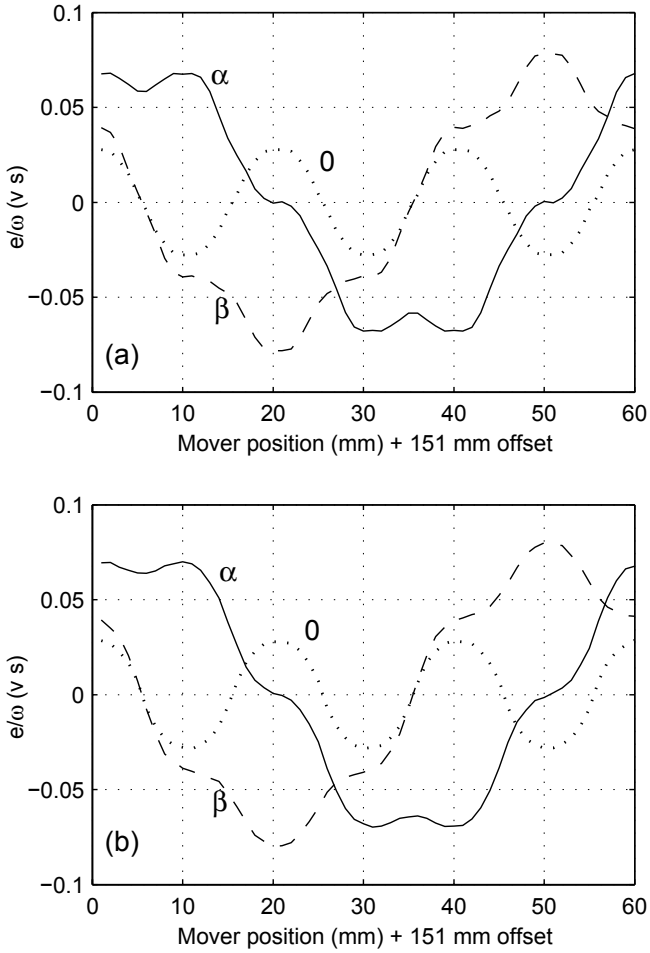

Fig. 6 Normalized EMF as a function of the position, a) by MEC, b) by FEA

transformed into the in αβ coordinates (i.e. Clarke Transformation). It was obtained by using the MEC model on one hand, and by using the FEA on the other. The inductances $L_{\alpha\alpha}$ and $L_{\beta\beta}$ obtained by the MEC model are shown in Fig. 5.a, and by FEA in Fig. 5.b. The inductance was derived with zero current. It is however also possible to analyze the inductance dependence on current by using this model.

Results were also obtained for the induced EMF. The normalized EMF $\mathbf{e}_{\alpha\beta 0}/\omega$ is shown in Fig. 6.a and Fig. 6.b as obtained by using the MEC model and the FEA model respectively (where ω is the electrical angular speed).

It should be remarked that the processing time for the FEA simulation took more than ten times the processing time for the MEC simulation. The MEC simulation was implemented in Matlab, in which the objective function is interpreted each iteration of the solver. This could be speed-up even more by compiling the objective function.

B. Dynamic MEC simulation compared with experimental results

In order to analyze the complete model, the injection of a high-frequency alternating voltage is tested. This test allows verifying the capability to use a sensorless method with signal injection as proposed in [8]. In this test, an alternating voltage is applied in the d-axis of an arbitrary reference frame γ,

$$\mathbf{u}^{\gamma} = \begin{bmatrix} a_C \cos(\omega_C t) \\ 0 \end{bmatrix} \tag{8}$$

where a_C is the amplitude of the injected voltage, and ω_C is the frequency. The resulting q-axis current, in the same reference frame, is bandpass filtered and demodulated as follows,

$$i_{dem} = i_q^{\gamma} \sin(\omega_C t) \tag{9}$$

If the motor presents magnetic saliencies, this signal will be position dependent and can be used to detect the mover's position [8]. As can be appreciated in Fig. 1, the mover has surface magnets. Consequently, the magnetic saliencies are mainly due to the saturation they produce in the stator.

For test purposes, the signal is injected at a constant reference frame angle γ, while the mover travels along the stator span at a low speed ($v = 0.156\,m/s$). The amplitude of the signal is $a_C = 80V$ and the frequency is 1 kHz. Simulation results of the demodulated signal i_{dem} are shown in Fig. 7

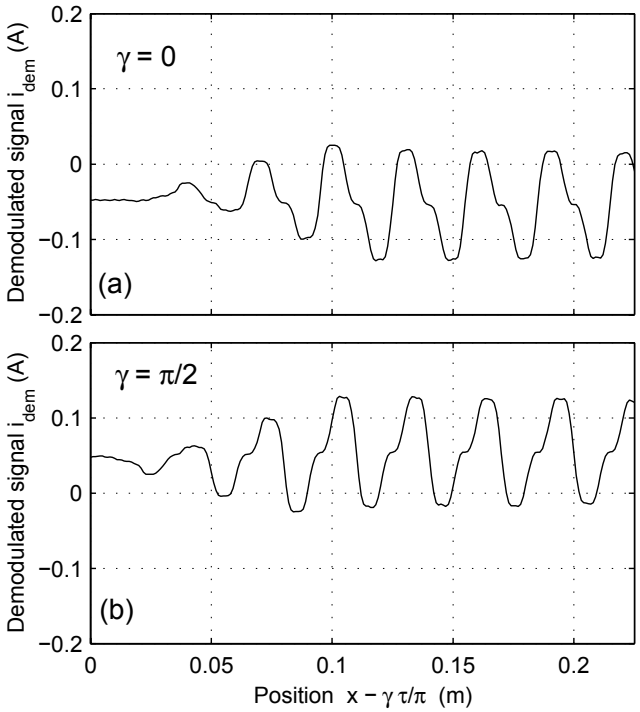

Fig. 7 Demodulated signal i_{dem} as a function of the position obtained by simulation, a) $\gamma = 0$, b) $\gamma = \pi/2$

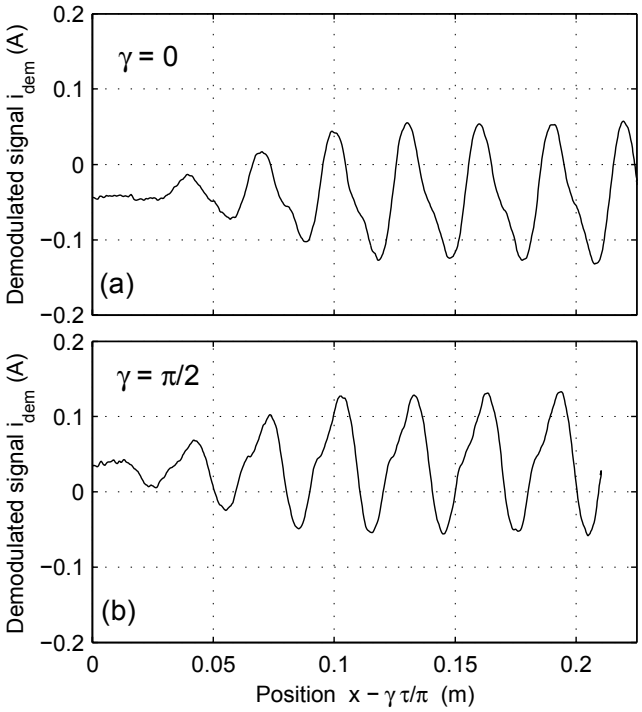

Fig. 8 Demodulated signal i_{dem} as a function of the position obtained by experimentation, a) $\gamma = 0$, b) $\gamma = \pi/2$

while in Fig.8 the experimental results for the same test are shown.

It can be appreciated in both figures that the signal i_{dem} presents an offset depending on the reference-frame angle γ. This offset, which can also be seen as a stationary saliency, will produce a perturbation in the position detection. However, as the reference frame angle γ is a known value, the offset can be compensated.

V. Conclusions

A dynamic model based on the Magnetic Equivalent Circuit (MEC) was derived for a Long-Stator Linear Synchronous motor. This allowed analyzing how sensorless methods would work on it. Characteristics like magnetic saliencies, due to the saturation that the permanent magnets produce in the stator, are well represented with this model. When the motor has wide yokes, this characteristic can be well modeled even including nonlinearity only in the stator teeth.

Results of the magnetostatic subsystem were compared with results obtained by Finite Element Analysis (FEA), showing good agreement between them. The complete MEC based model was also compared with experimental results, by injecting a high frequency voltage as used for sensorless methods. When comparing the obtained demodulated signal by simulation and by experimentation, slight differences raised. There are however, some known differences between the experimental setup and the model (e.g. the setup is arranged in a circular path, being therefore one wedge-shaped tooth per pole, while in the simulation all teeth are considered equal and rectangular). Nevertheless, with the proposed model it was possible to analyze the ability to apply a sensorless control method on the linear motor.

APPENDIX I

Equations of nodes $\mathbf{a_0}$, $\mathbf{a_1}$, $\mathbf{a_2}$, $\mathbf{a_3}$, a_4 and the equations of the teeth potentials, can be expressed in vector form, yielding respectively:

$$-\mathbf{I}_{(N-1)xN}\,\boldsymbol{\varphi}_{\mathbf{S}} + \mathbf{C_0}\,\mathbf{a_0} = \mathbf{0}_{(N-1)} \tag{10}$$

$$\boldsymbol{\varphi}_S + \mathbf{C_1}\,\mathbf{a}_1 - \mathbf{C_{11}}\,\mathbf{a_1} + \mathbf{C_{12}}\,\mathbf{a_2} = \mathbf{0}_N \tag{11}$$

$$-\boldsymbol{\varphi}_{\mathbf{PM}} - \mathbf{G}_{Ma}\left(\mathbf{a_2} - \mathbf{a_3}\right) + \mathbf{C_2}\,\mathbf{a_2} + \mathbf{C_{21}}\,\mathbf{a_1} - \mathbf{C_{22}}\,\mathbf{a_2} = \mathbf{0}_M \tag{12}$$

$$\mathbf{C_2} = \begin{bmatrix} -g_{ML1} & g_{ML1} & 0 & \cdots & 0 & 0 & 0 \\ g_{ML1} & -g_{ML1}-g_{ML2} & g_{ML2} & \cdots & 0 & 0 & 0 \\ \vdots & \vdots & \vdots & & \vdots & \vdots & \vdots \\ 0 & 0 & 0 & \cdots & g_{ML(M-2)} & -g_{ML(M-2)}-g_{ML(M-1)} & g_{ML(M-1)} \\ 0 & 0 & 0 & \cdots & 0 & g_{ML(M-1)} & -g_{ML(M-1)} \end{bmatrix}$$

$$\boldsymbol{\varphi}_{\mathbf{PM}} + \mathbf{G}_{Ma}\left(\mathbf{a}_2 - \mathbf{a}_3\right) + \mathbf{C}_3\,\mathbf{a}_3 - \mathbf{G}_{Mb}\left(\mathbf{a}_3 - \mathbf{I}_{\mathrm{M}}\,a_4\right) = \mathbf{0}_{\mathrm{M}} \tag{13}$$

$$\mathbf{1}_{1\mathrm{xM}}\mathbf{G}_{Mb}\mathbf{a}_3 - \mathbf{1}_{1\mathrm{xM}}\mathbf{G}_{Mb}\mathbf{1}_{\mathrm{Mx1}}a_4 = 0 \tag{14}$$

$$\mathbf{a}_1 - \mathbf{I}^{T}_{(\mathrm{N-1})\mathrm{xN}}\,\mathbf{a}_0 + \mathbf{F}_{\mathbf{S}} + \mathbf{f}_{ST}(\boldsymbol{\varphi}_{\mathbf{S}}) = \mathbf{0}_{\mathrm{N}} \tag{15}$$

where $\mathbf{I}_{\mathrm{X}}$ is the identity matrix of dimension X, $\mathbf{1}_{\mathrm{XxY}}$ is a XxY matrix of ones, $\mathbf{0}_{\mathrm{X}}$ is a column vector of dimension X,

$$\mathbf{I}_{(\mathrm{N-1})\mathrm{xN}} = \begin{bmatrix} 0 & 1 & 0 & \cdots & 0 \\ 0 & 0 & 1 & \cdots & 0 \\ \vdots & \vdots & \vdots & \ddots & \vdots \\ 0 & 0 & 0 & 0 & 1 \end{bmatrix}$$

$$\mathbf{C}_0 = \begin{bmatrix} -2g_Y & g_Y & 0 & \cdots & 0 & 0 & 0 \\ g_Y & -2g_Y & g_Y & \cdots & 0 & 0 & 0 \\ \vdots & \vdots & \vdots & \ddots & \vdots & \vdots & \vdots \\ 0 & 0 & 0 & \cdots & g_Y & -2g_Y & g_Y \\ 0 & 0 & 0 & \cdots & 0 & g_Y & -g_Y \end{bmatrix}$$

$$\mathbf{C}_1 = \begin{bmatrix} -g_L & g_L & 0 & \cdots & 0 & 0 & 0 \\ g_L & -2g_L & g_L & \cdots & 0 & 0 & 0 \\ \vdots & \vdots & \vdots & & \vdots & \vdots & \vdots \\ 0 & 0 & 0 & \cdots & g_L & -2g_L & g_L \\ 0 & 0 & 0 & \cdots & 0 & g_L & -g_L \end{bmatrix}$$

$$\mathbf{C}_{12} = \begin{bmatrix} g_{G11} & g_{G12} & \cdots & g_{G1M} \\ g_{G21} & & & g_{G2M} \\ \vdots & & \ddots & \vdots \\ g_{GN1} & g_{GN2} & \cdots & g_{GNM} \end{bmatrix}$$

$$\mathbf{C}_{21} = \mathbf{C}_{12}^{\mathbf{T}}$$

$$\mathbf{C}_{11} = \begin{bmatrix} \sum_{j=1}^{M} g_{G1j} & 0 & 0 & 0 \\ 0 & \sum_{j=1}^{M} g_{G2j} & 0 & 0 \\ \vdots & & \ddots & \vdots \\ 0 & 0 & 0 & \sum_{j=1}^{M} g_{GNj} \end{bmatrix} = \mathrm{diag}\left(\mathbf{C}_{12}\mathbf{1}_{\mathbf{Mx1}}\right)$$

$$\mathbf{C}_{22} = \begin{bmatrix} \sum_{i=1}^{N} g_{Gi1} & 0 & 0 & 0 \\ 0 & \sum_{i=1}^{N} g_{Gi2} & 0 & 0 \\ \vdots & & \ddots & \vdots \\ 0 & 0 & 0 & \sum_{i=1}^{N} g_{GiM} \end{bmatrix} = \mathrm{diag}\left(\mathbf{C}_{21}\mathbf{1}_{\mathbf{Nx1}}\right)$$

$$\mathbf{G}_{Ma} = \mathrm{diag}\left(\begin{bmatrix} g_{Ma1} & g_{Ma2} & \cdots & g_{MaM} \end{bmatrix}\right)$$

$$\mathbf{G}_{Mb} = \mathrm{diag}\left(\begin{bmatrix} g_{Mb1} & g_{Mb2} & \cdots & g_{MbM} \end{bmatrix}\right)$$

and $\mathbf{f}_{ST}$ is the elementwise function that relates tooth flux with its magnetic potential drop. Usually the magnetization curve is provided as a B vs. H table. From this table, a spline function can be implemented:

$$H = f_{Fe}(B) \tag{16}$$

From this function, the MMF can be related with the flux as follows:

$$F = f_{Fe}\left(\phi/(l_S b_S)\right)h = f_{ST}\left(\phi\right) \tag{17}$$

where l_S is the stack length, b_S is the tooth width, and h is the tooth height.

Equations (10)-(15) form the implicit function $\mathbf{f}_1$.

The equations of the equivalent circuit are rearranged to allow transformations (3) and (4) to be applied. Therefore, $\boldsymbol{\varphi}_S$ is solved from (11) yielding,

$$\boldsymbol{\varphi}_S = \left(\mathbf{C}_{11} - \mathbf{C}_1\right)\mathbf{a}_1 - \mathbf{C}_{12}\,\mathbf{a}_2 \tag{18}$$

Next, by substituting (18) into (10) and (15), and applying transformations (3) and (4), the equivalent circuit equations become,

$$-\mathbf{I}_{(\mathrm{N-1})\mathrm{xN}}\left(\left(\mathbf{C}_{11} - \mathbf{C}_1\right)\mathbf{a}_1 - \mathbf{C}_{12}\,\mathbf{a}_2\right) + \mathbf{C}_0\,\mathbf{a}_0 = \mathbf{0}_{(\mathrm{N-1})} \tag{19}$$

$$\boldsymbol{\lambda}_{\mathbf{S}} + \mathbf{w}'_{\mathbf{S}}\left(\mathbf{C}_1 - \mathbf{C}_{11}\right)\mathbf{a}_1 + \mathbf{w}'_{\mathbf{S}}\mathbf{C}_{12}\,\mathbf{a}_2 = \mathbf{0}_3 \tag{20}$$

$$-\boldsymbol{\varphi}_{\mathbf{PM}} + \mathbf{C}_{21}\,\mathbf{a}_1 - \left(\mathbf{C}_{22} + \mathbf{G}_{Ma} - \mathbf{C}_2\right)\mathbf{a}_2 + \mathbf{G}_{Ma}\mathbf{a}_3 = \mathbf{0}_{\mathrm{M}} \tag{21}$$

$$\boldsymbol{\varphi}_{\mathbf{PM}} + \mathbf{G}_{Ma}\mathbf{a}_2 - \left(\mathbf{G}_{Ma} - \mathbf{C}_3 + \mathbf{G}_{Mb}\right)\mathbf{a}_3 + \mathbf{G}_{Mb}\mathbf{1}_{\mathrm{Mx1}}a_4 = \mathbf{0}_{\mathrm{M}} \tag{22}$$

$$\mathbf{1}_{1\mathrm{xM}}\mathbf{G}_{Mb}\mathbf{a}_3 - \mathbf{1}_{1\mathrm{xM}}\mathbf{G}_{Mb}\mathbf{1}_{\mathrm{Mx1}}a_4 = 0 \tag{23}$$

$$\mathbf{a}_1 - \mathbf{I}^{T}_{(\mathrm{N-1})\mathrm{xN}}\,\mathbf{a}_0 + \mathbf{w}''_S\,\mathbf{i}_S + \mathbf{f}_{\mathbf{ST}}(\left(\mathbf{C}_{11} - \mathbf{C}_1\right)\mathbf{a}_1 - \mathbf{C}_{12}\,\mathbf{a}_2) = \mathbf{0}_{\mathrm{N}} \tag{24}$$

By offline solving the linear invariant subsystem, computational burden can be highly reduced for solving the DAE. Node potentials $\mathbf{a}_0$, $\mathbf{a}_3$ and a_4 can be solved from (19), (22) and (23), requiring only constant matrices to be inverted (taking into account that $\mathbf{C}_{11}$, $\mathbf{C}_{12}$, $\mathbf{C}_{21}$ and $\mathbf{C}_{22}$ are position dependent). After substituting the solved expressions for $\mathbf{a}_0$, $\mathbf{a}_3$ and a_4 into the remaining equations (20), (21) and (24), the implicit function $\mathbf{f}_2$ is obtained (eq. (5)).

ACKNOWLEDGMENT

This research results were attained with the assistance of the Alexander von Humboldt Foundation, Germany. The authors would like to thank for the support.

REFERENCES

[1] K. Rajashekara, A. Kawamura and K. Matsuse, *Sensorless Control of AC Motor Drives*, IEEE Press, New York, 1996.

[2] J. Holtz, "Perspectives of Sensorless AC Drive Technology", *in Proceedings of PCIM Europe*, Nürnberg, June 7-9, 2005, pp. 80-87.

[3] W. Limei and G. Qingding, "Sensorless control of permanent magnet linear synchronous motor based on nonlinear observer" *In Proceedings of the 8th IEEE International Workshop on Advanced Motion Control,* 2004. AMC'04, 25-28 March 2004. pp. 619-622.

[4] U.-H. Rieder, M. Schroedl „A Simulation Method for Analyzing Saliencies with Respect to Enhanced INFORM-Capability for Sensorless Control of PM Motors in the Low Speed Range including Standstill" *EPE 2005*. Dresden.

[5] V. Ostović, *Dynamics of Saturated Electric Machines*. Springer-Verlag. New York. 1989.

[6] J. Holtz and H Pan „Elimination of saturation effects in sensorless position-controlled induction motors" *IEEE Transactions on Industry Applications*, Vol. 40, No. 2, pp. 623-631.

[7] Shampine, Lawrence; Reichelt, Mark W.; Kierzenka, Jacek A. "Solving index-1 DAEs in MATLAB and Simulink". SIAM Rev. 41 (1999), no. 3, pp. 538-552.

[8] M. Linke, R. Kennel, J. Holtz, "Sensorless position control of permanent magnet synchronous machines without limitation at zero speed" *IEEE 28th Annual Conference of the Industrial Electronics Society IECON 02*, Vol. 1, 5-8 Nov. 2002 pp.674-679.